JOURNAL OF GEOPHYSICAL RESEARCH, VOL. 109, D07102, doi:10.1029/2003JD003986, 2004

Corrrection published 25 March 2005

Assessment of current passive-microwave- and infrared-based satellite rainfall remote sensing for flood prediction

Faisal Hossain and Emmanouil N. Anagnostou

Department of Civil and Environmental Engineering, University of Connecticut, Storrs, Connecticut, USA

Received 18 July 2003; revised 19 December 2003; accepted 12 February 2004; published 8 April 2004.

[1] The adequacy of current passive-microwave-(PM)- and infrared-(IR)-based satellite rainfall retrieval and sampling for flood prediction of a medium-sized watershed is investigated. On the basis of Tropical Rainfall Measuring Mission (TRMM) Precipitation Radar rainfall measurements, rain retrieval error parameters for PM and IR sensors are derived. PM rain retrievals are inferred from the overland component of the TRMM Microwave Imager (TMI) rain estimation algorithm, while IR retrievals are obtained from hourly PM-calibrated IR rain fields, which are part of a variable rainfall product (VAR) array produced at NASA/GSFC. A probabilistic error model is developed for satellite-based precipitation measurements on the basis of retrieval error parameters in this simulation study. The PM rain detection ability was found to be significantly more sensitive than that of IR while the successful no-rain detection probabilities were found to be 93% and 88%, respectively. The IR retrieval was found to give false alarm rain rates about twice as large as that of PM. The PM sensor constellation comprised two Special Sensor Microwave Imagers (SSM/I) (F14 and F15), the TMI, and the Advanced Microwave Sensing Radiometer (AMSR-E). It was found that current PM sampling is associated with flood prediction uncertainty approximately 50–100% higher than that of a canonical 3-hourly sampling planned for the Global Precipitation Measurement (GPM) mission. The comparatively greater limitation in capturing the correct space-time rain structure by IR retrievals had the effect of increasing the error in predicting the time of peak runoff when merging was performed with PM retrievals. It was found that a reduced standard error (<100%) in IR retrieval combined with a higher probability of rain detection (POD) (>0.90) can make IR retrievals useful in reducing uncertainty in the prediction of peak runoff. To reduce the error in time to peak, further improvement, such as reduction in the IR retrieval's false alarm rates coupled with an even higher POD, may be necessary. In terms of overall runoff volume, combined moderate improvements in POD and error variance of current IR retrieval algorithms are sufficient for the reduction of prediction uncertainty. *INDEX TERMS:* 1821 Hydrology: Floods; 1854 Hydrology: Precipitation (3354); 1860 Hydrology: Runoff and streamflow; 1869 Hydrology: Stochastic processes; 1894 Hydrology: Instruments and techniques; *KEYWORDS:* rainfall retrieval, sampling, passive microwave, infrared, flood prediction uncertainty

Citation: Hossain, F., and E. N. Anagnostou (2004), Assessment of current passive-microwave- and infrared-based satellite rainfall remote sensing for flood prediction, *J. Geophys. Res.*, *109*, D07102, doi:10.1029/2003JD003986.

1. Introduction

[2] Advancements in space-based precipitation observation systems that originated nearly three decades ago [*Griffith et al.*, 1978] have enabled us to track the fate of precipitation in the hydrologic cycle through improved understanding of its variability. With the increased availability and quality of precipitation observations from space it is now possible to assimilate these estimates in hydrologic models to provide flood prediction over regions with poor in situ data. This is important as a substantial portion of floods takes place in regions that are remote or that lack the financial resources to be adequately covered by ground stations. In such cases, space-based rainfall estimates are the sole source of rain input to hydrological models. Since precipitation is the single most important determinant of the state of surface runoff, it is therefore important to understand how errors in satellite retrieval manifest themselves as flood prediction uncertainty.

[3] Global Precipitation Measurement (GPM), which is a mission to be launched by the international community by 2009, envisions a large constellation of passive microwave (PM) sensors to provide global rainfall products at scales ranging from 3 to 6 hours and spatial resolution of 100 km^2 [*Smith*, 2001; *Bidwell et al.*, 2002; *Flaming*, 2002; S. Yuter et al., Error and uncertainty in precipitation measurements, *GPM Monitor*, Feb. 2003, available at http://gpm.gsfc.

0148-0227/04/2003JD003986$09.00

nasa.gov/Newsletter/february03/index.htm]. These resolutions offer tremendous opportunities to address the flood prediction problem of local ungauged watersheds over the globe. Nevertheless, satellite rainfall retrieval is subject to errors caused by various factors ranging from infrequent sampling to the high complexity and variability in the relationship of the measurement to precipitation parameters. The presence of such errors in remote sensing of rainfall can potentially lead to high uncertainties in runoff simulation [*Winchell et al.*, 1998; *Borga et al.*, 2000; *Hossain et al.*, 2004a, 2004b]. A study by *Smith* [2001] has revealed that the current (pre-GPM era) PM sensors collectively have their maximum revisit times exceeding 9 hours over the tropics. Unfortunately, this is a region where a large number of ungauged watersheds exist. Half-hourly infrared (IR) rainfall estimates from geostationary platforms could potentially reduce the flood prediction uncertainty during such infrequent PM revisit intervals. However, the weak physical connection of IR cloud top observations to precipitation processes offers indirect relationships to surface rainfall variability, which are associated with significant uncertainty at high spatial and temporal resolutions [*Arkin and Meisner*, 1987]. Consequently, this study seeks to assess how current satellite rainfall retrievals and sampling frequencies affect flood prediction uncertainty. This understanding is important in the identification of aspects that could make future satellite missions such as the GPM useful for flood prediction applications.

[4] To understand the error propagation, it is important to realize that the error due to the three major sources of uncertainty: retrieval, sampling, and the hydrological modeling system, are all intimately linked and cannot be decomposed into simple additive components in flood prediction uncertainty [*Borga et al.*, 2000; *Borga*, 2002; *Hossain et al.*, 2004a, 2004b]. Past satellite rainfall studies have concentrated on the rain retrieval uncertainty issue for large spatial scales and temporal accumulations (daily, monthly, and yearly) using a limited number of error statistics (*Griffith et al.* [1978], *Arkin and Meisner* [1987], *Negri and Adler* [1993], *Tsonis et al.* [1996], *Huffman* [1997], *Xu et al.* [1999a, 1999b], and *Todd et al.* [2001], among others). These statistics are quite useful in assessing the use of satellite data for large-scale climatological or water management studies [*Guetter et al.*, 1996; *Nijssen et al.*, 2001]. However, the averaging introduced at coarse resolution smoothes the small-scale variability of measurement error, which can have nonlinear effects in the runoff simulation parameters of a flood event (e.g., the time and magnitude of the peak runoff). A recent study by *Nijssen and Lettenmaier* [2004] attempted to quantify the sole effect of precipitation sampling error on the prediction of land surface processes at the scale of large continental river basins. They reported a strong sensitivity of streamflow prediction error to the size of the drainage area. However, their study provides insufficient assessment toward the evaluation of the utility of current satellite retrievals for flood prediction because of the nonrepresentation of the retrieval uncertainty, which is known to interact intimately with the sampling error. It also appears that the macroscale hydrologic models that have been developed to study land-atmospheric processes and interactions in this regard have not yet been fully assessed in terms of their sensitivity to the detailed structural properties of satellite rainfall estimation error [*O'Donnell et al.*, 2000; *Nijssen et al.*, 2001; *Rhoads et al.*, 2001; *Nijssen and Lettenmaier*, 2004].

[5] This study aims at assessing the use of current PM and IR satellite rainfall remote sensing in flood prediction. The study builds upon the recent work by *Hossain et al.* [2004b] (hereinafter referred to as HAD04), who investigated the adequacy of a canonical 3-hourly and 6-hourly PM sampling for flood prediction using simulated satellite retrievals. The objectives of the present study are to (1) compare the effect of current PM sampling frequencies to the planned canonical 3-hourly GPM era in terms of flood prediction uncertainty for a mid-sized watershed; (2) study the effect of storm morphology on the uncertainty of flood prediction driven by satellite rainfall data; and (3) investigate potential improvements associated with the combination of IR rain estimates with PM retrievals.

[6] In section 2 we describe the study area, hydrologic model, and data. In section 3 we describe the formulation and tuning to actual data of the statistical model used to simulate PM and IR rain retrievals from hypothetically true rain processes. In section 4, we present the simulation experiment, results, and discussion of findings. Section 5 contains the conclusions and discusses proposed extensions of this study.

2. Study Area, Hydrologic Model, and Data

[7] The watershed chosen for this study (named Posina) is located in northern Italy, close to Venice (Figure 1, right panel). Posina has an area of 116 km^2 and altitudes ranging from 2230 to 390 m at the outlet (Figure 1, left panel). Within a radius of 12 km from the center of the watershed there is a network of 11 rain gauges reporting hourly rain accumulations, 7 of which are closer to the watershed, providing representative estimates of the basin-averaged hourly rainfall rates (hereinafter referred to as "accumulated reference rain rate"). The annual precipitation accumulation is estimated to be in the range of 1600–1800 mm. Posina is 68% forested, and saturation-excess is the main rainfall-runoff generation mechanism. Further details about the study area, including its terrain characteristics and rain climatology, are given by *Borga et al.* [2000].

[8] The rainfall-runoff model TOPMODEL [*Beven and Kirkby*, 1979] was chosen to simulate the rainfall-runoff processes of floods in the Posina watershed. It is a semi-distributed watershed model that can simulate the variable source area mechanism of storm runoff generation and incorporates the effect of topography on flow paths. This model makes a number of simplifying assumptions about the runoff generation process that are thought to be reasonably valid in this wet and humid environment. The model is premised on the following two assumptions: (1) that the dynamics of the saturated zone can be approximated by successive steady state representations; and (2) that the hydraulic gradient of the saturated zone can be approximated by the local surface topographic slope. Detailed background information of the model and applications is given by *Beven et al.* [1995]. The model has been applied in the study region and found adequate to simulate the rainfall-runoff transformation processes of the watershed [*Borga et al.*, 2000; *Hossain et al.*, 2004a]. As with many other

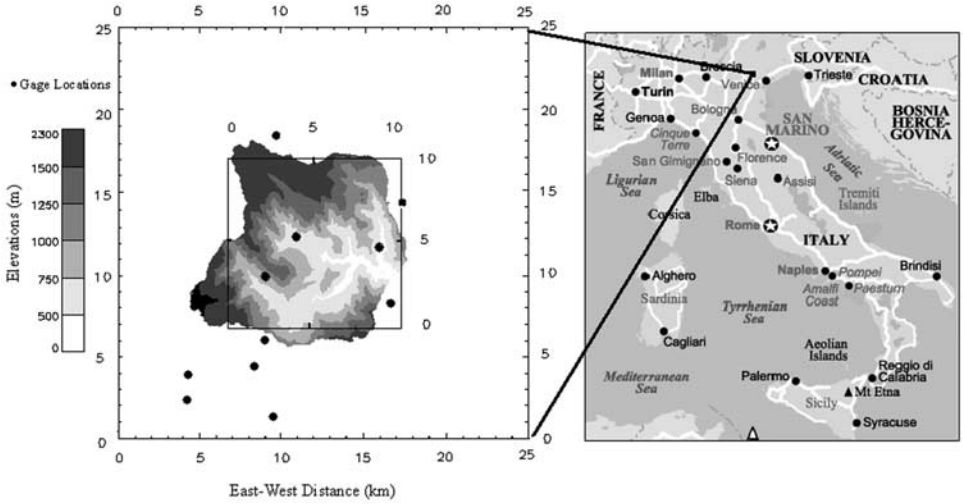

Figure 1. Geographic location of Posina watershed (right panel) and watershed elevation map (left panel) overlaid by the rain gauge network locations (in solid circles). The inner rectangle represents a 10×10 km^2 PM satellite pixel over the watershed, while the larger box is a 25×25 km^2 pixel for representing IR retrievals.

TOPMODEL applications, the topographic index ln (a/tan β) is used as an index for hydrological similarity, where a is the area draining through a point, and tan β is the local surface slope. In this study, the derivation of the topographic index from a 20-m grid size digital terrain model utilized the multiple-flow-direction algorithm by *Quinn et al.* [1991, 1995]. The rainfall input to the model was lumped (basin-averaged). The generated runoff was routed to the main channel using an overland flow delay function. The main channel routing effects are considered using an approach based on an average flood wave velocity for the channel network.

[9] A series of 15 widespread storm events (3–7 days long) that took place from 1987 to 1997 were studied (Table 1). Shorter-duration intense precipitation events (<2 days) have been excluded from this study, as they would be most affected by the infrequent PM sampling. Generalizations of findings from this study are therefore

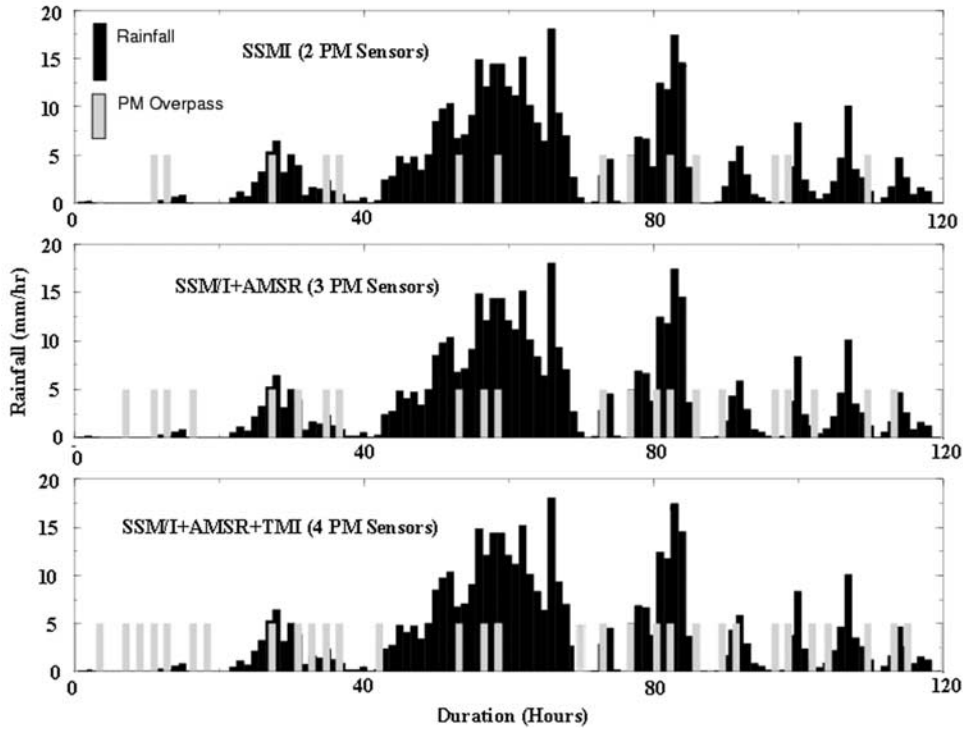

Figure 2. An example of simulated overpasses by the assumed complement of four PM sensors for storm 9 (October 1992). The assumed constellation comprises SSM/I-F14, SSM/I-F15, TMI, and AMSR-E.

Table 1. Statistical Summary of Storm Events With the Simulated PM Sampling Overpasses of the Assumed Complement of Four PM Sensors

		Rainfall Statistics						PM Sampling (2 SSM/I + AMSR-E + TMI)		
	Date (Month Year)	Duration, hours	Rain Fraction, %	Mean Conditonal Rain Rate, mm/h	Std. Dev., mm/h	CV,[a] %	Maximum Discharge, m^3/s	Sampling Coverage, hours	Maximum Revisit Time, hours	Mean Revisit Time, hours
1	08 1987	72	34.0	3.90	5.8	148	54.40	14	11	5.1
2	10 1987	96	40.8	2.80	2.7	96	75.72	21	11	4.3
3	07 1989	96	29.0	3.20	2.9	91	31.49	21	11	4.3
4	11 1990	96	35.8	2.80	2.9	103	64.37	21	11	4.3
5	12 1990	108	40.1	3.61	3.9	108	76.41	25	11	4.5
6	03 1991	72	32.3	2.49	2.9	115	32.59	14	11	5.1
7	10 1991	84	44.4	3.85	4.5	170	117.40	17	11	4.6
8	04 1992	120	58.3	1.35	2.3	107	56.89	26	11	4.4
9	10 1992	120	86.7	4.24	4.5	107	192.50	26	11	4.4
10	12 1992	144	36.3	1.94	1.9	99	41.60	32	11	3.9
11	09 1993	132	61.5	2.98	3.5	116	49.40	30	11	4.2
12	11 1994	72	55.0	3.65	4.1	112	106.90	14	11	5.1
13	10 1996	96	85.4	3.65	3.2	87	156.50	21	11	4.3
14	11 1996	120	81.7	1.84	2.3	124	70.80	26	11	4.4
15	12 1997	84	76.0	1.78	2.3	128	70.26	17	11	4.6

[a]Coefficient of variation.

limited to flood events lasting longer than 2 days and for medium-sized (50–500 km^2) watersheds driven by saturation-excess runoff production processes. The storms studied here are the outcome of cyclogenesis in the surrounding regions enhanced by orographic lifting in the mountainous Alpine terrain when the moisture-laden clouds from the Mediterranean travel northward [*Bacchi et al.*, 1996]. The first seven columns of Table 1 describe the basic features of the storm morphology. We present the storm duration, rain fraction, mean conditional rain rate, standard deviation, and coefficient of variation (CV: standard deviation normalized by the mean). In the last three columns of Table 1, we present the characteristics of the simulated PM sampling for these storm events. The assumed constellation comprised four PM sensors (TMI, SSM/I-F14, SSM/I-F15, and AMSR-E). The inclusion of TMI makes the implicit assumption that the watershed be hypothetically located within ±40° latitudes. The constellation's sampling pattern over the watershed was identified on the basis of a satellite-tracking system maintained by NASA (http://earthobservatory.nasa.gov/MissionControl/overpass.html) and from real sensor data of SSM/I-F14, SSM/I-F15, and TMI. We first identified the mean of the sampling pattern for a typical 7-day period (the maximum storm duration in our database) for a few locations, each of 0.1-degree resolution, distributed uniformly within the tropics. We then assumed this mean weekly sampling pattern to be representative for the description of hypothetical PM overpasses for the storm events under study. Figure 2 shows the sampling pattern identified in this fashion for a particular storm (storm 9 in Table 1) by the assumed complement of four PM sensors. The overall sampling pattern appears to be consistent with that identified by *Smith* [2001], who has reported a maximum revisit time exceeding 9 hours within the tropics. The "sampling coverage" in Table 1 indicates the number of hours with available PM rainfall retrievals. Also in Table 1 we show the "maximum and mean revisit time," which is the maximum and mean time between successive PM overpasses, respectively. The maximum revisit time was found to be invariably equal to 11 hours for all storm cases.

3. Satellite Rainfall Error Model

3.1. Model Formulation

[10] Our motivation for the formulation of a satellite rainfall error model (SREM) is the need to fully characterize the retrieval error of satellite sensors at high resolutions. It is obvious that as the space scales and timescales become smaller, the sensor's precipitation measurement error characteristics become more complex and random. In this study, we adopted the probabilistic error model originally developed by HAD04. The error model is schematically presented as a flowchart in Figure 3, and details are discussed below.

[11] The approach is to simulate statistical realizations of satellite (PM and IR) rainfall retrievals by corrupting a more accurate measurement of rainfall. In this study, the most accurate measurement of rainfall available constituted the basin-averaged hourly accumulated rainfall derived from the dense network of rain gauges within and around the Posina basin (earlier labeled as "accumulated reference rainfall"). Satellite retrievals, though, represent almost instantaneous rainfall fields. To quantify the error of instantaneous rain rates in representing accumulated hourly rainfall, we define two error characteristics: (1) the error in rain detection and (2) conditional error. The probability of detection of instantaneous rain rate POD_{INST} is used to define the detection error:

$$POD_{INST} = \text{Prob}\{R_{REF-INST} > 0 \mid R_{REF-ACCU} > 0\}, \quad (1)$$

where $R_{REF\text{-}INST}$ represents realizations of an instantaneous area-averaged reference rain rate value and $R_{REF\text{-}ACCU}$ is the accumulated reference rainfall of the corresponding hour.

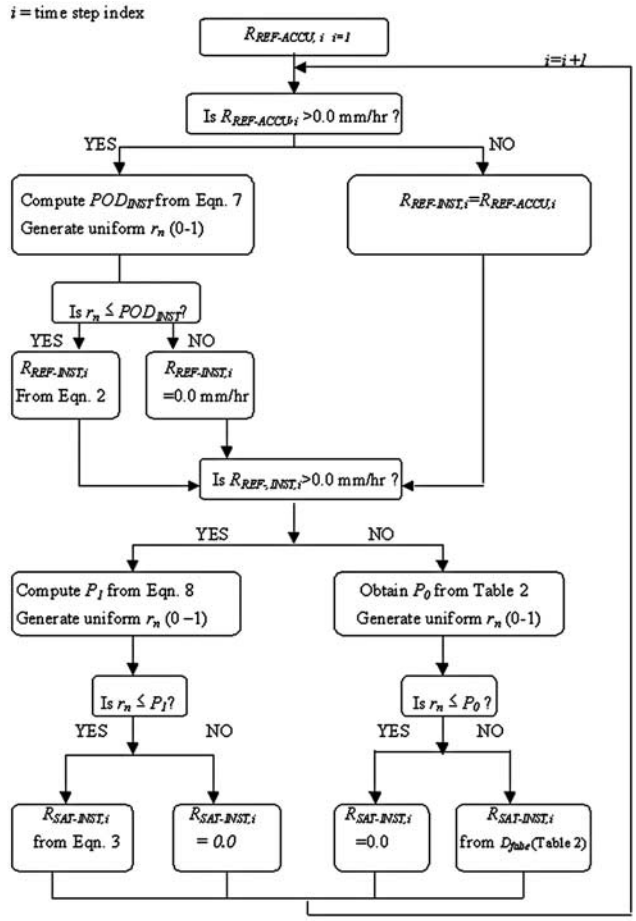

Figure 3. Satellite rainfall error model (SREM) algorithmic structure. The r_n is a randomly generated number from the uniform [0–1] probability distribution.

The conditional error $E_{\text{INST-ACCU}}$ of $R_{\text{REF-INST}}$ with respect to $R_{\text{REF-ACCU}}$ is defined as

$$E_{\text{INST}-\text{ACCU}} = R_{\text{REF}-\text{ACCU}}/R_{\text{REF}-\text{INST}}. \tag{2}$$

Because of the multiplicative nature of the error the statistical distribution of $E_{\text{INST-ACCU}}$ is considered to be lognormal, with mean and variance components defined as $\text{MU}_{\text{INST-ACCU}}$ and $S_{\text{INST-ACCU}}$, respectively. The above error-modeling framework is used to statistically generate instantaneous reference rain rates $R_{\text{REF-INST}}$ from the hourly accumulated area-averaged reference rainfall values $R_{\text{REF-ACCU}}$ determined from gauges; this is discussed later in this section.

[12] An instantaneous satellite rain retrieval, on the other hand, may exhibit one of the following possible outcomes: (1) When it actually rains, the satellite retrieval can be nonzero (successful rain detection) or zero (false no-rain detection), while (2) when it does not rain, the satellite retrieval can also be zero (successful no-rain detection) or nonzero (false rain detection).

[13] We define the successful rain detection probability P_1 as a function of $R_{\text{REF-INST}}$. The functional form is identified through calibration with actual data as discussed in the following section. The false no-rain detection is derived from P_1 as $(1 - P_1)$. The successful no-rain detection P_0 is the unitary probability that satellite retrieval is zero when $R_{\text{REF-INST}}$ is zero, which is also determined from actual data. The false rain detection probability is then derived from P_0 as $(1 - P_0)$. A probability density function D_{false} is introduced to characterize the probability distribution of the satellite retrieval in false rain detection. This function is also identified through calibration on the basis of actual sensor data.

[14] The nonzero instantaneous satellite rain retrieval $R_{\text{SAT-INST}}$ is statistically related to corresponding nonzero instantaneous reference rain rate $R_{\text{REF-INST}}$ as

$$R_{\text{SAT}} = R_{\text{REF}-\text{INST}}.\ \varepsilon_S, \tag{3}$$

where the multiplicative satellite error parameter ε_s is assumed lognormally distributed. The lognormality of the distribution is justified by the nonnegative property of ε_s. A log transformation of the log (R_{SAT}) − log $(R_{\text{REF-INST}})$ statistical relationship transforms the error ε_s to a Gaussian deviate ε with $N(\mu, \sigma)$ statistics, where μ and σ are the mean and standard deviation, respectively. To determine the multiplicative mean MU_{INST} and standard deviation S_{INST} of ε_s, the following conversion is used in terms of μ and σ:

$$\text{MU}_{\text{INST}} = \exp\left(\mu + 0.5\sigma^2\right), \tag{4}$$

$$S^2_{\text{INST}} = \left[\exp\left(\sigma^2\right) - 1\right]\exp\left(2\mu + \sigma^2\right). \tag{5}$$

The error parameter ε (hereinafter also referred to as "log-error") can be spatially and temporally autocorrelated. Only temporal autocorrelation is considered in this study because the watershed scale is represented by a single PM satellite retrieval pixel (~100 km^2, see Figure 1, left panel). A lag-one autocorrelation function was used to model the correlated error sequence, which for a Gaussian random variable, leads to the following equations for the propagation of μ and σ^2:

$$\mu_i = \mu + (\rho)(\varepsilon_{i-1} - \mu), \sigma_i^2 = \sigma^2\left(1 - \left(\rho^2\right)\right), \tag{6}$$

where time index i represents discrete hourly time step while ρ^2 is the lag-one autocorrelation of ε. The previous study by HAD04 had shown evidence of the runoff error being insensitive to the lag-one autocorrelated rain retrieval error for 3- and 6-hourly sampling scenarios; hence ρ^2 was constrained to a fixed value of 0.4 in this study.

[15] The SREM operation is summarized in the flowchart of Figure 3. When at a certain hour i the hourly accumulated area-averaged reference rainfall is nonzero ($R_{\text{REF-ACCU},i} > 0$), we use equations (1) and (2) to generate the realization of an instantaneous reference rain rate $R_{\text{REF-INST},i}$. Namely, a Bernoulli trial is conducted to model the POD_{INST} by generating a uniform U[0, 1] random number r_n. If r_n is less than POD_{INST} (which is determined as a function of $R_{\text{REF-ACCU},i}$), an instantaneous reference rain rate $R_{\text{REF-INST},i}$ is calculated on the basis of equation (2) by randomly generating a lognormally distributed deviate LN [$\text{mu}_{\text{INST-ACCU}}$, $S_{\text{INST-ACCU}}$], representing $E_{\text{INST-ACCU}}$. Next, when the instantaneous reference rain rate is nonzero ($R_{\text{REF-INST},i} > 0$), the

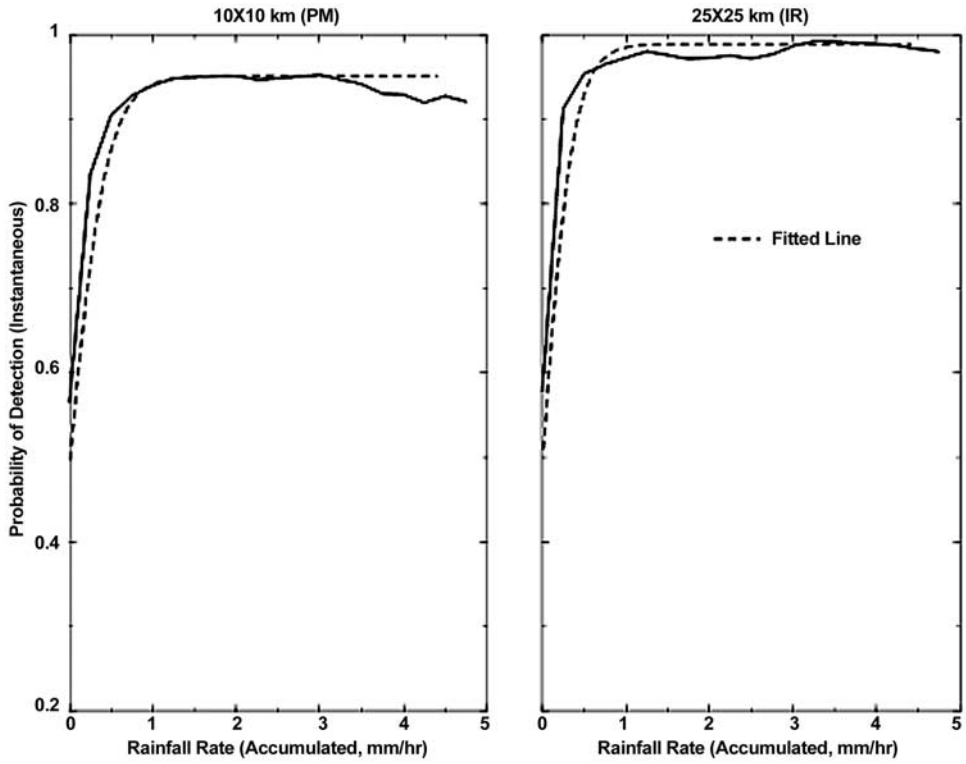

Figure 4. Probability of detection POD_{INST} of 10-min (representing instantaneous) reference rain rate as a function of hourly accumulated reference rainfall. The dashed lines are the best fits to the data.

satellite error model (SREM) decides as to whether the satellite rainfall is zero or not through another set of Bernoulli trials. If the uniform U[0,1] random number r_n generated is less than P_1 (which is determined as a function of $R_{\text{REF-INST},i}$), then the instantaneous satellite retrieval $R_{\text{SAT},i}$ is nonzero and modeled through equation (3). Otherwise, $R_{\text{SAT},i}$ is assigned a zero value. Similarly, during a nonrainy hour ($R_{\text{REF-INST},i} = 0$), a Bernouilli trial is used again to decide as to whether the satellite rainfall will be zero or nonzero. If the uniformly random deviate r_n is less than P_0, then $R_{\text{SAT},i}$ is assigned a zero value. Otherwise, the nonzero satellite rainfall value is determined through random sampling on the basis of the false alarm probability density D_{false} function.

3.2. SREM Calibration

[16] Having mathematically formulated the algorithm for SREM, the next step is to calibrate the model parameters on the basis of actual data at the sensor resolution. We seek to determine the values and/or functional forms of (1) POD_{INST}, $MU_{INST\text{-}ACCU}$, and $S_{INST\text{-}ACCU}$ parameters of the instantaneous rainfall representativeness error and (2) the P_1, P_0, D_{false}, MU_{INST}, and S_{INST} parameters of SREM.

[17] To evaluate the POD_{INST}, $MU_{INST\text{-}ACCU}$, and $S_{INST\text{-}ACCU}$ parameters, we used six months of high-resolution (1 min) rainfall data from a gauge network in the area; the storm intensities and durations were of similar magnitudes to the storms studied herein. We created time series of 10-min rain accumulations at 10×10 and 25×25 km^2 area averages by averaging the gauge rainfall reported within each domain size to make it representative of the PM and IR retrieval scales. Within the PM (10×10 km^2) domain there were 4 gauges, while the IR domain had a total of 8 (inclusive of all the gauges in the PM domain) gauges. A study reported by *Habib and Krajewski* [2002] has shown that a 5–10-min accumulation can be considered representative of an instantaneous remote sensing measurement at 4×4 km^2 grid; in our case, this space scale-timescale similarity may be representative of even larger time integrations given the coarser spatial resolution of both IR and PM retrievals. Figure 4 shows the dependency of POD_{INST} on $R_{\text{REF-ACCU}}$. We observe that at hourly accumulated rainfall values beyond 1 mm/h the 10-min sample will have probability greater than 95% to report rainfall. A sigmoid function of the form shown in equation (7) (below) appeared a statistically good fit to model POD_{INST}.

$$\text{POD}_{\text{INST}}(R_{\text{REF-ACCU}}) = \frac{1}{A_{\text{ACCU}} + \exp(-B_{\text{ACCU}} R_{\text{REF-ACCU}})}. \quad (7)$$

[18] The other error parameters, $MU_{INST\text{-}ACCU}$ and $S_{INST\text{-}ACCU}$, controlling the conditional error are reported in Table 2. To generate instantaneous reference rain rates for the PM retrieval, hourly accumulated reference rainfall values were computed from an average of 7 gauges located within a 10×10 km^2 grid surrounding the basin and subsequently corrupted by the representative error model comprising equations (1) and (2). To generate corresponding instantaneous reference rain rates for the IR retrieval, the hourly accumulated reference rainfall values were computed from the entire network of

Table 2. Mean Error Model Parameters Calibrated for PM (2A12) and IR (3B41RT) Sensor Retrievals on the Basis of Coincident TRMM Precipitation Radar Rainfall Fields

	2A12 (10×10 km^2)	3B41RT (25×25 km^2)
A_{ACCU} (A_{INST})	1.05 (1.0)	1.01 (1.35)
B_{ACCU} (B_{INST})	4.5 (3.5)	5.5 (1.0)
λ	0.9	0.5
$MU_{INST\text{-}ACCU}$ (MU_{INST})	1.0 (1.27)	1.0 (1.52)
$S_{INST\text{-}ACCU}$ (S_{INST})	0.24 (0.94)	0.19 (1.51)
Lag-one correlation ρ^2	0.40	0.40
No-rain detection probability P_0	0.93	0.88

11 gauges that are within the 25×25 km^2 grid area (see Figure 1, left panel, for a schematic of the gauge network configuration).

[19] We used as common reference (i.e., our "truth") for PM and IR retrievals coincident rain profile estimates from TRMM Precipitation Radar (PR) [*Kummerow et al.*, 2000]. The PR estimates are based on a radar profiling retrieval that is superior to any overland passive microwave technique [*Iguchi et al.*, 2000]. The primary aspects of the retrieval are the precipitation classification, which is facilitated by the high-vertical-resolution (250 m) reflectivity profile measurements, and an inversion algorithm that is controlled by a surface reference technique for path-integrated attenuation and a reflectivity-to-rainfall relationship with parameters differentiated for convective and stratiform rain regimes [*Iguchi et al.*, 2000; *Meneghini et al.*, 2000]. Ground validation studies on PR have shown high correlation (>0.9) and low (<7%) systematic differences with rain-gauge-calibrated ground radar rainfall estimates [*Anagnostou and Morales*, 2002; *Liao et al.*, 2001].

[20] The calibration exercise was performed in three distinct geographic regions with TRMM coverage: United States (35°N to 15°N and 100°–70°W), Africa (10°N to 10°S and 10°–40°E), and the Amazon Basin (0°N to 20°S and 60°–30°W). We selected a period of three months (May–July 2002) to determine the PM retrieval error model parameters, while for the IR retrieval we selected a period of 1 year (February 2002 to January 2003). The PM retrieval was evaluated on the basis of matched TRMM PR and TMI rainfall products aggregated at 10×10 km^2 resolution relevant to the size of the watershed. The TMI rainfall product used in this study is the 2A12 TRMM product computed with the Goddard profiling algorithm (GPROF) [*Kummerow et al.*, 2001]. A fairly optimistic assumption made in this study is that GPROF retrieval errors for SSM/I and AMSR-E sensor observations are comparable to those of the TMI sensor. In terms of IR retrievals, we used the hourly PM-calibrated variable IR rainfall product (VAR) produced by multisatellite precipitation analysis (MPA) [*Huffman et al.*, 2003]. This data product is operationally known as 3B41RT. The IR retrieval error was evaluated at 25×25 km^2 resolution on the basis of coincident PR scans that are within a maximum time window of 15 min of the nominal scan time of the IR image, in a fashion similar to *Negri et al.* [2002]. Although the IR scale is larger than the size of the watershed, this is the smallest scale at which a global hourly IR rain product is currently available for flood prediction.

[21] In Figure 5 we show a representative example of matched instantaneous TMI and IR rain map with PR over Africa. The convection indicated by the PR seems to be well detected by the TMI (leftmost panel, Figure 5). For the IR there may be a possibility of a spatial offset and overestimation in the presence of convection when compared to the PR (rightmost panel, Figure 5). This can possibly be due to the anvil of convective cirrus clouds (a likely scenario in Africa) being displaced from the active convective elements by vertical shear or mesoscale dynamics [*Huffman et al.*, 2003]. IR retrievals are also likely to underestimate the peak rain rate and delay the time of peak for warm rain systems.

[22] Figure 6 shows the sensor's rain detection probability within rain rate ranges of 0–10 mm/h determined from instantaneous sensor data previously described. Again, a sigmoidal function of the form shown similar to equation (7) (equation (8) below) appeared to be a statistically good fit to the above rain detection probabilities. We argue for a sigmoidal function as it offers a physically consistent and convenient model for rain detection because of its bounded nature within the realistic 0–1 probability levels and because it is often difficult to identify the most

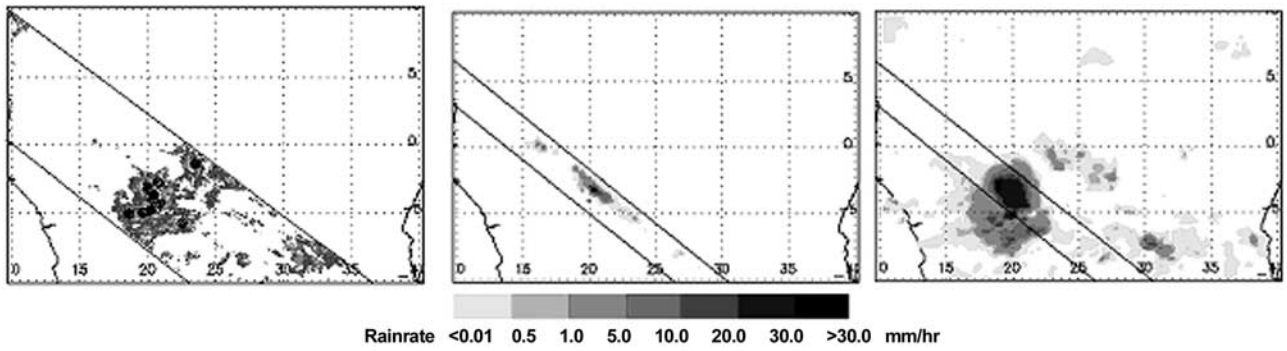

Figure 5. An example of matched TMI- (2A12), IR- (3B41RT), and TRMM-PR- (2A25) retrieved rain maps over central Africa. (left) TMI (orbit 24225); (middle) PR (orbit 24225); (right) IR (1300 UTC), on 13 February 2002. PR and IR are shown at 25×25 km^2 resolution.

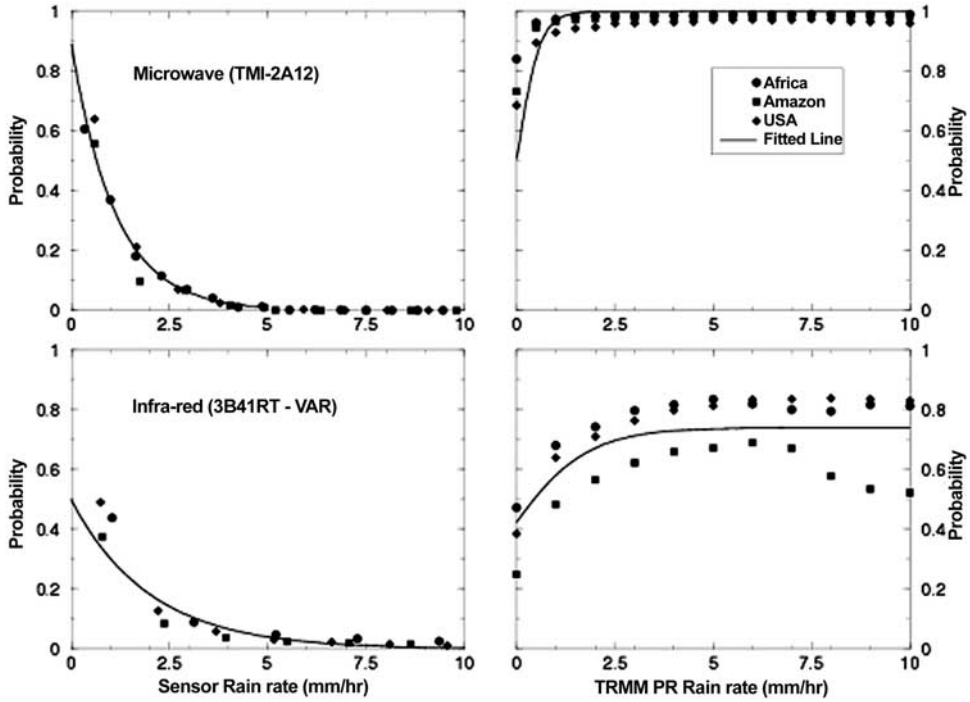

Figure 6. Probabilities of rain detection (right panels) and probability distributions of rain rates in false alarms (left panels) for PM (upper panels) and IR (lower panels) retrievals. These experimental results are determined on the basis of coincident TRMM PR overland rainfall data around the globe. The solid lines are best fits to the data.

representative functional form that fits the entire range of data (especially for IR retrievals).

$$P_1(R_{\mathrm{REF-INST}}) = \frac{1}{A_{\mathrm{INST}} + \exp(-B_{\mathrm{INST}} R_{\mathrm{REF-INST}})}. \quad (8)$$

The inverse of coefficient A_{INST} serves to indicate the maximum possible rain detection probability within the above range of reference instantaneous rain rates. Coefficient B_{INST} indicates the sensitivity of the retrieved rain detection ability to the magnitude of the reference instantaneous rain rate. The calibrated values of all the error parameters for SREM are shown in Table 2. As shown in Figure 6 (right panels), PM rain detection ability is significantly more sensitive than that of IR. At instantaneous reference rain rates beyond 2.5 mm/h, PM rain detection converges to nearly 1, while the IR rain detection remains below 80%. The IR successful no-rain detection probability P_0 is found to be 88%, while the corresponding PM is 93% (a difference of 5%).

[23] The probability distribution function of the falsely detected instantaneous rain rates D_{false} was found to be exponential, $D_{\mathrm{false}}(R_{\mathrm{SAT}}) = \lambda \exp\{-\lambda R_{\mathrm{SAT}}\}$, for both PM and IR retrievals (see left panels of Figure 6). The fitted λ values for PM and IR retrievals are shown in Table 2. We observe that the IR retrieval is likely to give false alarm rain rates about twice as large as those from PM. In Table 2 we also summarize the two statistics characterizing the multiplicative conditional instantaneous rain retrieval error: mean $\mathrm{MU}_{\mathrm{INST}}$ and standard deviation S_{INST}. These statistics are the mean over the three large regions chosen for calibration. An IR retrieval standard error about 1.5 times that of PM observed in our calibration study appears to be consistent with what has been previously reported in the literature (see HAD04 for details).

4. Simulation Experiment

[24] Using a global optimization routine [*Duan et al.*, 1992], the TOPMODEL parameters were calibrated for each of the 15 storm events at 1-hourly and 3-hourly time steps using hourly accumulated reference rainfall and observed runoff. The gauge-based simulated hydrographs from the hourly calibrated TOPMODEL parameters were considered as reference runoff. To account for the relative effect of the hydrologic model's inherent prediction error, we also considered the observed versus reference runoff difference for three hydrologic parameters: peak runoff PR, time to peak runoff TP, and runoff volume RV. Table 3 summarizes the normalized absolute error of the reference runoff $\mathrm{NAE}_{\mathrm{REF}}$ for each storm event. Multiple runs of the hydrologic model, each having as rain input a random realization of the satellite-retrieved rain process simulated from SREM, were then performed and compared to reference runoff to statistically assess the effect of satellite retrieval error and sampling error on flood prediction uncertainty. As shown in Table 3, the hydrologic modeling error is considerably lower than that due to rainfall error alone. Nevertheless, in evaluating the satellite retrieval error statistics we considered both rain input and modeling error; this is discussed later in this section. For the assessment of the PM retrievals, which are available at coarse temporal sampling (>3 hours), hydrologic simulations were performed at 3-hourly time

Table 3. Hydrologic Modeling Error of TOPMODEL Based on Observed Runoff Versus Reference Runoff Differences[a]

	Normalized Absolute Error NAE_{REF}		
Storm	Runoff Volume	Peak Runoff	Time to Peak Runoff
1	0.038	0.310	0.080
2	0.027	0.083	0.000
3	0.008	0.043	0.000
4	0.022	0.048	0.000
5	0.035	0.016	0.075
6	0.210	0.540	0.056
7	0.098	0.110	0.038
8	0.099	0.062	0.031
9	0.083	0.232	0.000
10	0.309	0.019	0.000
11	0.069	0.129	0.017
12	0.007	0.071	0.000
13	0.128	0.072	0.011
14	0.119	0.025	0.016
15	0.115	0.089	0.051
Mean	0.091	0.123	0.025

[a]Normalized absolute error $NAE_{REF} = |X_{obs} - X_{ref}|/X_{obs}$.

steps using the relevant calibrated TOPMODEL parameters. For the assessment of the combined PM-IR retrievals, which are available at hourly scale because of the frequent IR data, hydrologic simulations were performed at the hourly time step using the hourly calibrated TOPMODEL parameters. For each storm event an ensemble of 20,000 realizations of synthetic satellite precipitation retrievals from SREM were propagated through the hydrologic model to derive an equal number of simulated hydrographs for computation of error statistics in runoff simulation.

[25] The following hydrologic error parameters are assessed in this study: (1) normalized mean absolute error in peak runoff PR, (2) normalized mean absolute error in time to peak TP, and (3) normalized mean absolute error in runoff volume RV, defined as

$$\begin{aligned}
\text{error in PR} &= \frac{1}{N_{\text{sim}}}\sum_{i=1}^{N_{\text{sim}}}\left|\frac{\text{peak runoff}_i - \text{peak runoff}_{\text{REF}}}{\text{peak runoff}_{\text{REF}}}\right| \\
&\quad + \text{NAE}_{\text{REF_PR}}, \\
\text{error in TP} &= \frac{1}{N_{\text{sim}}}\sum_{i=1}^{N_{\text{sim}}}\left|\frac{\text{time to peak}_i - \text{time to peak}_{\text{REF}}}{\text{time to peak}_{\text{REF}}}\right| \\
&\quad + \text{NAE}_{\text{REF_TP}}, \\
\text{error in RV} &= \frac{1}{N_{\text{sim}}}\sum_{i=1}^{N_{\text{sim}}}\left|\frac{\text{runoff volume}_i - \text{runoff volume}_{\text{REF}}}{\text{runoff volume}_{\text{REF}}}\right| \\
&\quad + \text{NAE}_{\text{REF_RV}},
\end{aligned} \tag{9}$$

where N_{sim} is the total number of simulation runs (20,000), subscript i indicates the simulation index, and subscript "REF" implies the hydrologic parameter that was derived from reference runoff. The second term in equation (9), NAE_{REF_X}, represents the hydrologic modeling error for each hydrologic parameter X (PR, TP, and RV) due to reference runoff.

4.1. Assessment of PM Retrievals

[26] We first assess the PM retrieval alone. In this case, the instantaneous rain rate fields are assumed constant between successive PM overpasses, which is a reasonable

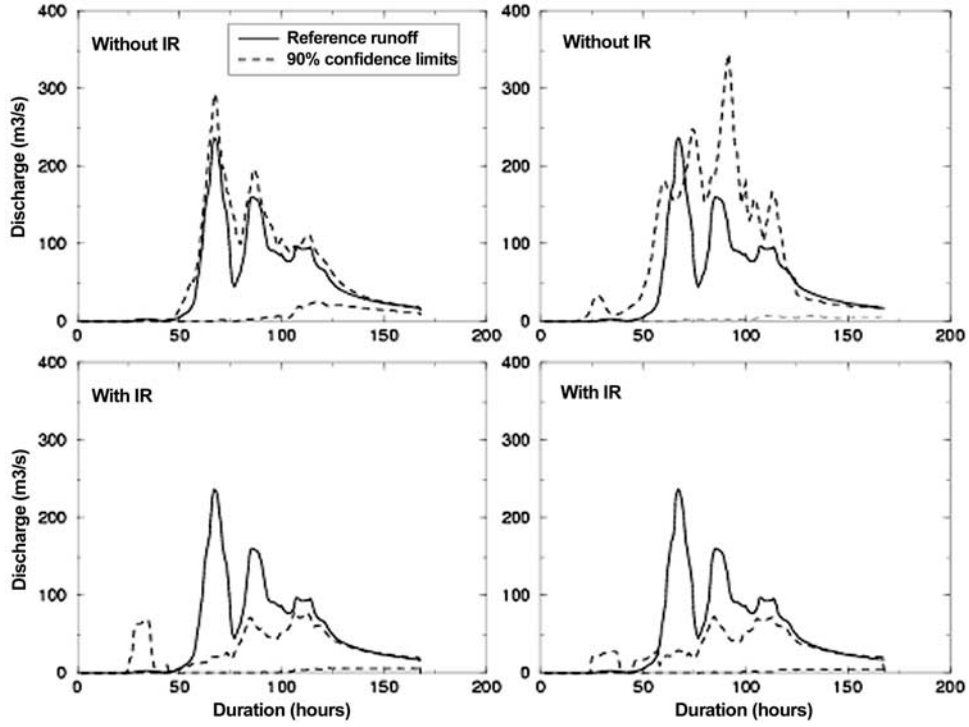

Figure 7. Flood prediction uncertainty (5% and 95% upper/lower quantiles) of storm 9 (October 1992) for the GPM-based 3-hourly sampling (left) and current PM sampling (right). Upper panels are based on PM retrievals, and lower panels are based on the merged IR-PM rain products.

Table 4. Runoff Prediction Error Ratio ER Values of PM Retrievals for the 15 Storm Events Evaluated for the Current PM Sampling Scenario

	Error Ratio ER		
Storm	Peak Runoff	Time to Peak Runoff	Runoff Volume
1	1.09	1.01	1.13
2	1.31	1.77	1.46
3	6.29	1.67	3.47
4	1.01	2.72	1.23
5	1.23	1.16	1.17
6	1.07	1.04	1.19
7	1.31	3.09	1.38
8	1.11	3.56	1.30
9	1.12	1.09	1.13
10	1.22	1.00	1.17
11	1.04	1.27	1.69
12	1.14	7.04	1.59
13	1.15	1.08	1.19
14	1.16	4.09	1.24
15	2.70	1.01	2.12
Mean	1.52	2.17	1.50

scenario for real-time operation. As the TOPMODEL was run using 3-hourly time steps, simulated runoff was interpolated at hourly intervals by a polynomial function. Because the first overpass by a PM sensor may occur at any time during a storm event, we also considered all possible sampling start times (rounded off to the closest hour) for the examined storms. For this purpose, we shifted the start of the PM sampling up to 11 hours, which was the maximum revisit time during an event (see Table 1, column 10).

[27] The same procedure was followed to determine the error statistics in terms of the above runoff parameters for the planned GPM-based 3-hourly canonical PM sampling. Although GPM revisit time intervals would vary between 1 and 6 hours (with an average revisit time of 3 hours), we have assumed an idealized scenario of 3-hourly canonical sampling. The 3-hourly error statistics were used to normalize the error statistics determined for the current PM-based prediction as

$$\text{error statistics ratio (ER)} = \frac{\text{runoff error statistics (current PM sampling)}}{\text{runoff error statistics (3-hourly sampling)}}. \quad (10)$$

These error ratios ER, determined for the PR, TP, and RV parameters, are used to quantify the factor by which the current PM sampling scenario is more uncertain than the planned GPM 3-hourly sampling in terms of flood prediction. We argue that ERs are more informative than using absolute errors in understanding the implications of the retrieval and sampling error in runoff.

[28] The upper panels of Figure 7 show the PM-based hydrographs along with the 90% confidence limits for one of the storms in our database (storm 9). The runoff prediction uncertainty of the current PM retrievals (right panel) appears to be higher (approximately 50%) than those associated with the 3-hourly PM sampling (left panel). The uncertainty in peak runoff was nearly 350 m^3/s (compared to the 300 m^3/s for the 3-hourly sampling), while the time to peak tended to be overestimated by about 20 hours. This can be explained by the high revisit times (~11 hours) between successive PM overpasses, which can completely misinterpret the peak rainfall rates of a storm (see Figure 2, lowermost panel). Table 4 shows the ER values of the runoff parameters for all 15 storms. The mean ER values of peak runoff, time to peak runoff, and runoff volume are 1.52, 2.17, and 1.50, respectively. Overall, the flood prediction uncertainty based on the current PM retrieval and sampling is found to be higher than what would be achieved by the planned 3-hourly GPM sampling in the range of 50–100%. An interpretation of this is that the GPM can be expected to be more reliable for flood prediction than current PM sensors but significant uncertainty would still persist as indicated in Figure 7.

[29] Figure 8a shows the response of storm morphology to flood prediction uncertainty associated with current PM retrieval and sampling. In the upper left panel, the impact of storm duration to error in time to peak is evident. As storm durations become longer (from 3 to 7 days) the time to peak runoff is predicted with less error (a reduction from 220% to 30% is observed). This is explained by the fact that the PM satellite sampling effect becomes less important as storm duration increases. We also observe that as the rain fraction (%) increases, the error in runoff volume reduces moderately (Figure 8a, upper right panel). It is noted that because of the high PM rain detection probability, as the hours during a storm event associated with rain increase, the error for a PM sensor to retrieve the storm's total rainfall accumulation decreases. There is insignificant sensitivity observed in the mean conditional rain rate (lower left panel, Figure 8a) and variability of rain rate (lower right panel, Figure 8a) to the error in runoff volume. When the response of the storm morphology to flood prediction uncertainty for the current PM sampling is compared to the planned GPM 3-hourly sampling (shown in Figure 8b), the following two notable effects are observed. First, the hydrologic error statistics (mainly error in time to peak and runoff volume) are lowered by an average of 10–30%. Second, the overall sensitivity of the four storm morphological parameters on the flood prediction uncertainty appears to diminish, as there are no obvious gradients and widespread scatter observed in Figure 8b. Consequently, the increased sampling in GPM should allow more consistent flood prediction than current PM sampling for storm events whose morphological properties are within the domain analyzed herein.

4.2. Assessment of Combined PM-IR Retrievals

[30] In this section, we assess the utility of merging IR retrievals with PM. We used simulated (through SREM) hourly IR rainfall retrievals to fill up the gaps between successive simulated PM retrievals and repeated the runoff simulation experiment on the basis of the framework described in section 4.1. There are two major distinctions to be highlighted in the application herein: (1) The time step used in the hydrologic model simulation is now hourly, and (2) the hourly accumulated reference rainfall for the IR retrieval pertains to averaged rainfall over a 25 × 25 km^2 grid area surrounding the Posina basin as we discussed before in section 3.2 (see also Figure 1, left panel). Results of this simulation experiment are used to determine an error

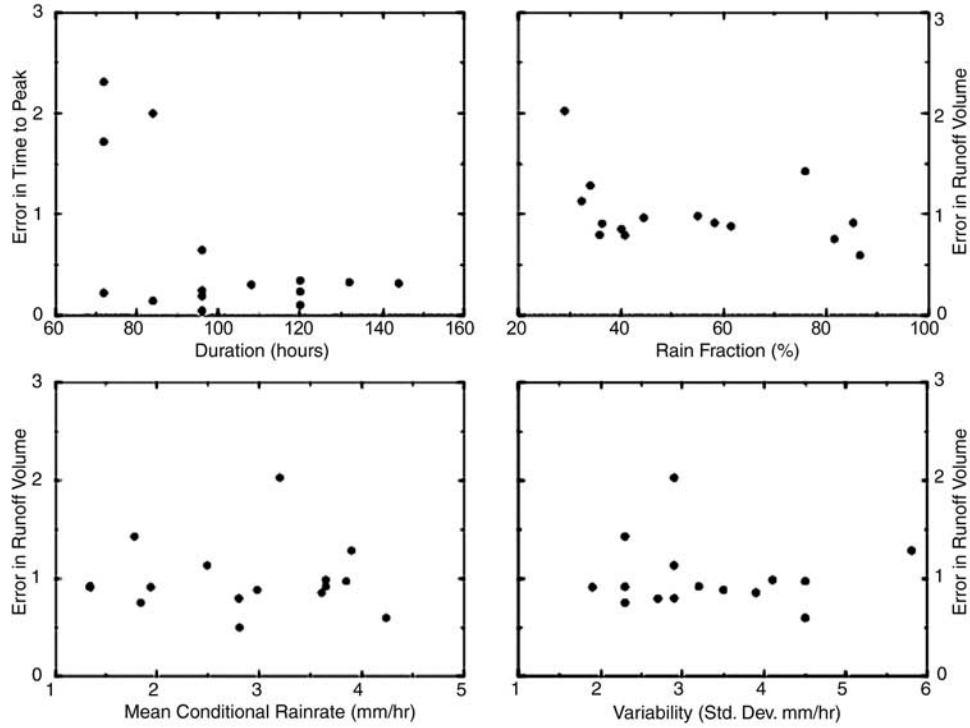

Figure 8a. Effect of storm morphology on the uncertainty of flood prediction driven by current PM retrieval sampling scenarios. Upper left panel: error in time to peak versus storm duration; upper right panel: error in runoff volume versus rain fraction; lower left panel: error in runoff volume versus mean conditional rain rate; lower right panel: error in runoff volume versus standard deviation of conditional rain rate.

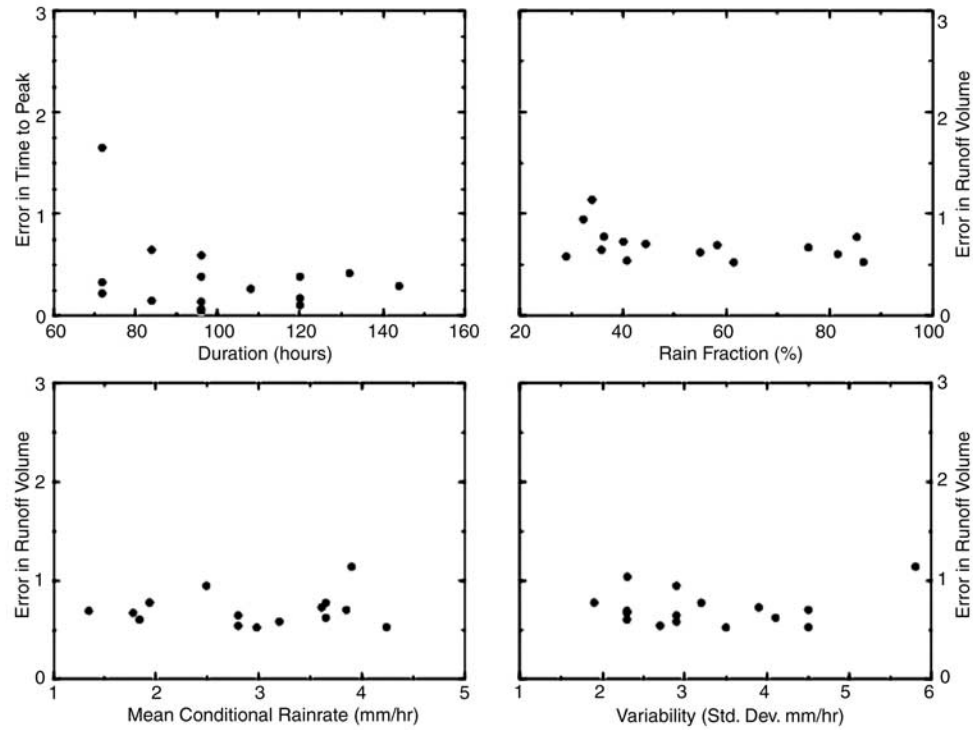

Figure 8b. Same as in Figure 8a, but for flood predictions driven by the GPM-based 3-hourly PM sampling scenario.

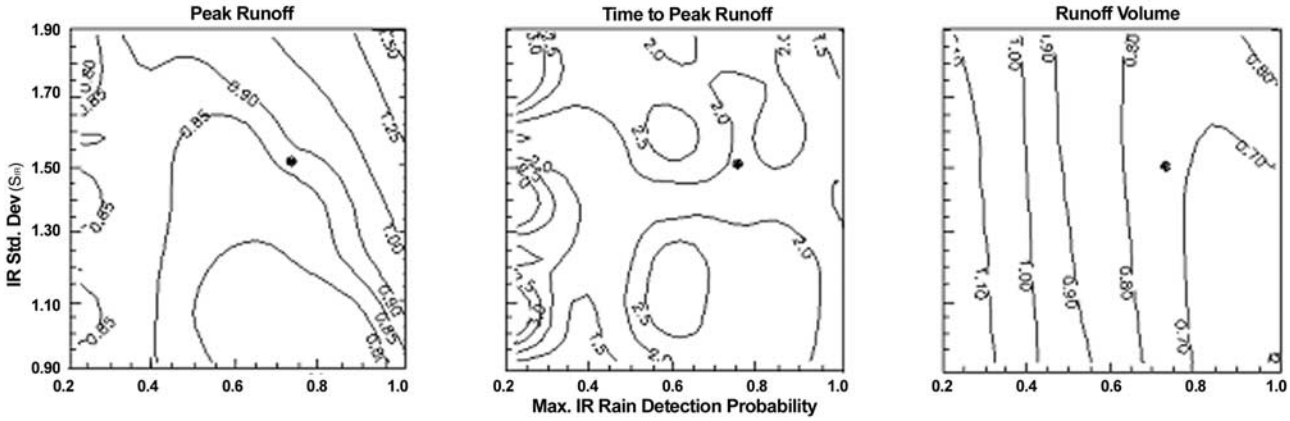

Figure 9a. Contours of merging ER values representing the relative runoff prediction error of the combined PM-IR rain products to PM retrieval alone (current PM sampling scenarios), for various levels of IR rain estimation accuracy (S_{IR} versus maximum IR rain detection probability). (left) Merging ERs in peak runoff; (middle) merging ERs in time to peak runoff; (right) merging ERs in runoff volume. The solid circles represent the retrieval level of the current IR algorithm (3B41RT).

parameter named the "merging error ratio" (merging ER) and defined as follows:

$$\text{merging ER} = \frac{1}{\text{nstorm}} \sum_{i=1}^{\text{nstorm}} \cdot \frac{\text{runoff error statistics (merged PM-IR retrievals)}_i}{\text{runoff error statistics (PM retrievals)}_i}. \tag{11}$$

Here nstorm is equal to 15 (the total number of storm events), with i being the storm index. Merging ER values are determined for all three runoff parameters. A merging ER value of less than 1 indicates that the merging of IR with PM retrievals reduces the overall uncertainty in the associated runoff parameter compared to the stand-alone use of PM rain retrieval input.

[31] The example shown in Figure 7 (lower panels) indicates that the use of IR retrievals with current performance statistics can, for a catastrophic flood event like storm 9, worsen the flood prediction uncertainty for both the GPM and current PM sampling scenarios. Even though the 90% confidence limits are narrower when filling sampling gaps with IR, the reference runoff is enveloped only sparsely by these bounds (for example the first peak is completely missed for storm 9). This indicates that the hydrologic model had lost its predictive accuracy through the use of the IR retrieval. Our findings in this study indicate that the worsening in flood prediction for storm 9 can be attributable to the relatively lower rain detection accuracy of IR retrievals at finer scale, which results in a net underestimation of total rain volume compared to that by the four PM retrievals (upper right panel, Figure 7). Although a portion of this underestimation may have been compensated for by the higher IR false alarm rates, the inaccurate temporal characterization of rain fluxes renders the corresponding estimation of runoff in time similarly erroneous. In the next section, we shall analyze in detail the response of PM-IR retrieval in runoff, considering all 15 storm events jointly.

[32] In Figure 9a we present the impact of combined PM-IR retrievals for various hypothetical levels of IR retrieval accuracy and current PM sampling. As IR measurement accuracy can be sensitive to scale and the retrieval technique, a range of possible IR uncertainty levels are expected in future algorithm improvements. Keeping the PM retrieval error characteristics, the IR's D_{false} and probability of no-rain detection P_0 fixed at the calibrated values (shown in Table 2), the IR's maximum rain detection probability was covaried with the IR multiplicative conditional retrieval error standard deviation S_{IR}. The variation of maximum rain detection probability was performed from 0.2 (very low rain detection probability) to 1.0 (an optimistic scenario where IR equals the maximum detection probability of PM) by varying parameter A_{INST} in equation (8) (0.75 forms the IR rain detection level for the 3B41RT). The error standard deviation S_{IR} was covaried from 0.9 (a fairly optimistic scenario comparable to PM, see Table 2) to 1.90 (a pessimistic scenario) (1.51 forms the current level of S_{IR}). The covariation of these two IR retrieval parameters was assessed in terms of their reduction in flood prediction uncertainty by evaluating the merging ER parameter (equation (11)). The temporal correlation ρ^2 of IR error was fixed to 0.4.

[33] Several distinct features are worth noting from Figure 9a. While merging ER in both peak runoff and runoff volume decreases below 1 in the optimistic regions of IR retrieval performance (Figure 9a, leftmost and rightmost panels), it was always higher than 1 for time to peak (Figure 9a, middle panel). It seems that IR retrievals' high false alarm rate (nearly twice as much of the PM) coupled with its relatively lower probability of no-rain detection P_0 obscured the positive effect of improving rain detection and retrieval error variance on the prediction of time to peak runoff. On the other hand, IR retrievals are found to reduce uncertainty moderately by 15–20% in peak runoff prediction when they are associated with high rain detection levels ($P_{1\ IR} > 0.90$) and with comparably lower conditional error standard deviation ($S_{IR} < 1.0$) (Figure 9a, leftmost panel). For a similar amount of error reduction in runoff volume

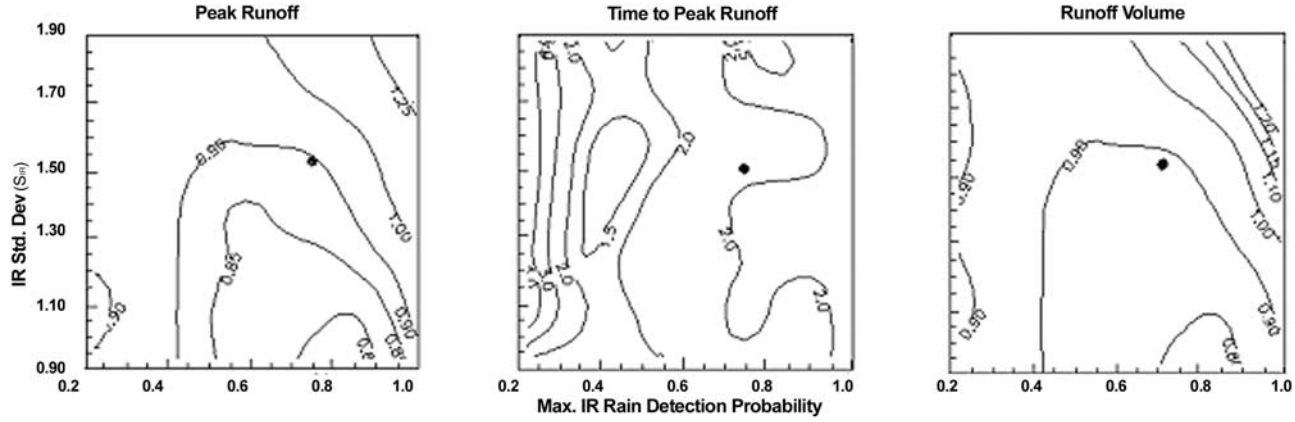

Figure 9b. Same as in Figure 9a, but for the GPM-based 3-hourly sampling scenario.

simulation, a lesser IR rain detection probability ($P_{1\ IR} > 0.70$) seems necessary. The stronger gradients along the axis of rain detection probability (abscissa of rightmost panel) indicate that the runoff volume error is more responsive to improvements in IR rain detection than the other two hydrologic parameters (PR and TP).

[34] In Figure 9b we present the impact of combined PM-IR retrievals for varying levels of IR retrieval accuracy associated with the 3-hourly GPM sampling scenario. While we observe a pattern of error interaction qualitatively similar to that presented for the current PM sampling, there is a distinctive aspect emerging from the increased sampling frequency in GPM. The merging ER values are about 20–30% higher than those of current PM sampling for both the peak runoff and runoff volume parameters (see leftmost and rightmost panels of Figure 9b). This indicates that with an improved PM sampling, the benefit of combining IR with PM retrievals to reduce flood prediction uncertainty is an expected reduction of 20–30%. This agrees with a previous study by HAD04, where it was found that runoff error for a canonical 3-hourly PM sampling was 30–50% lower than that of a 6-hourly PM sampling. For the time to peak parameter we still observe that combined PM-IR retrievals would increase the prediction uncertainty compared to using solely PM-based predictions.

5. Conclusions

[35] Hydrologic assessment of satellite rainfall retrievals for flood prediction warrants the recognition that as the space scales and timescales become smaller, the sensor's precipitation detection and retrieval accuracy become increasingly more complex. This study revealed that current PM retrieval and sampling scenarios can be 50–100% more uncertain than the planned GPM-era 3-hourly sampling scenario in terms of flood prediction for medium-sized watersheds. The merging of IR with PM retrievals on the basis of current retrieval error characteristics showed that it would worsen flood prediction uncertainty, especially in terms of the time to peak prediction, and for catastrophic storm events. Considering that the accuracy of IR retrievals varies by scale and retrieval technique and that improvements are expected in new algorithms, various levels of its measurement uncertainty were assessed here in terms of the reduction in flood prediction uncertainty when merged with PM retrievals. It was found that for certain levels (some of them very optimistic for an IR retrieval scheme at a fine resolution) of rain detection efficiency and conditional retrieval error variability of IR rain estimates can lead to significant reduction of prediction uncertainty in terms of runoff volume and peak runoff parameters. No error reduction in time to peak was achieved, however. Probably, to reduce the error in time to peak, further improvement, such as a reduction in IR retrieval's false alarm rates coupled with an even higher rain detection ability, may be necessary.

[36] Results from this study are limited to major floods resulting from long-lasting storms (>2 days) and saturation-excess runoff generation mechanisms from medium-sized mountainous watersheds (50–500 km^2). Mountainous basins at these scales are prone to high flood risks, while satellite observations for many of those regions are probably the only data source for measuring rainfall. Nevertheless, the results of this study cannot be generalized to other scales and runoff generation mechanisms. For example, the work needs to be expanded to larger basins and other land surface environments (e.g., vegetated versus dry regions and/or basins dominated by infiltration excess runoff) to better understand the interactions of precipitation error with hydrology. The study herein highlighted the need for improving satellite retrieval error characteristics to achieve improved hydrologic forecasts. Recent techniques have sought such improvements in IR rain estimation accuracy through pattern recognition of cloud features [*Xu et al.*, 1999a], assimilation of lightning information [*Morales and Anagnostou*, 2003; *Chronis et al.*, 2004], and assimilation of microwave information [*Todd et al.*, 2001], to name a few. Similarly, PM retrievals continue to evolve regularly in terms of new overland techniques [*McCollum and Ferraro*, 2003] and improved sampling and resolutions as we transition to the GPM era. It is worthwhile, therefore, to understand the effect of scale on the precipitation measurement error from a host of single-sensor and multisensor retrievals and how this propagates in hydrologic prediction. Furthermore, short-duration storms and larger-size watersheds need to be studied to understand the temporal sampling problem and the aspect of spatial variability of satellite measurement error in runoff prediction. These are some of the many aspects that need to be addressed to achieve more meaning-

ful applications of satellite rainfall observations to flood hydrology.

[37] **Acknowledgments.** This study was supported by NASA TRMM and GWEC projects. The first author was supported by a NASA Earth System Science Graduate Student Fellowship. The authors acknowledge and appreciate the constructive comments from three anonymous reviewers. Marco Borga of the University of Padua, Legarno, Italy, provided the watershed and storm data for the study. The infrared and TRMM data were provided by the NASA/Goddard Space Flight Center's Laboratory for Atmospheres and TSDIS on the basis of a data-mining exercise with NASA.

References

Anagnostou, E. N., and C. Morales (2002), Rainfall estimation from TOGA radar observations during LBA field campaign, *J. Geophys. Res.*, *107*(D20), 8068, doi:10.1029/2001JD000377.

Arkin, P. A., and B. N. Meisner (1987), The relationship between large-scale convective rainfall and cold cloud over Western Hemisphere during 1982–1984, *Mon. Weather Rev.*, *115*, 51–74.

Bacchi, B., R. Ranzi, and M. Borga (1996), Statistical characterization of spatial patterns of rainfall cells in extratropical cyclones, *J. Geophys. Res.*, *101*(D21), 26,277–26,286.

Beven, K. J., and M. J. Kirkby (1979), A physically-based variable contributing area model of basin hydrology, *Hydrol. Sci. J.*, *24*(1), 43–69.

Beven, K. J., R. Lamb, P. Quinn, R. Romanowicz, and J. Freer (1995), TOPMODEL, in *Computer Models of Watershed Hydrology*, edited by V. P. Singh, pp. 627–668, Water Resour. Publ., Highlands Ranch, Colo.

Bidwell, S., J. Turk, M. Flaming, C. Mendelsohn, D. Everett, J. Adams, and E. A. Smith (2002), Calibration plans for the Global Precipitation Measurement, paper presented at Joint 2nd International Microwave Radiometer Calibration Workshop and CEOS Working Group on Calibration and Validation, Comm. on Earth Obs. Satell., Barcelona, Spain, 9–11 Oct.

Borga, M. (2002), Accuracy of radar rainfall estimates for streamflow simulation, *J. Hydrol.*, *267*, 26–39.

Borga, M., E. N. Anagnostou, and E. Frank (2000), On the use of real-time radar rainfall estimates for flood prediction in mountainous basins, *J. Geophys. Res.*, *105*(D2), 2269–2280.

Chronis, T., E. N. Anagnostou, and T. Dinku (2004), High-frequency estimation of thunderstorms via satellite infrared and a long-range lightning network in Europe, *Q. J. R. Meteorol. Soc.*, in press.

Duan, Q., S. Sorooshian, and V. K. Gupta (1992), Effective and efficient global optimization for conceptual rainfall-runoff models, *Water Resour. Res.*, *28*, 1015–1031.

Flaming, M. (2002), Requirements of the Global Precipitation Mission, paper presented at IGARSS 2002 (International Geoscience and Remote Sensing Symposium), Inst. of Electr. and Electron. Eng., Toronto, Ont., Canada, 24–28 June .

Griffith, G. C., W. L. Woodley, and P. G. Grube (1978), Rain estimation from geosynchronous satellite imagery-visible and infrared studies, *Mon. Weather Rev.*, *106*, 1153–1171.

Guetter, A. K., K. P. Georgakakos, and A. A. Tsonis (1996), Hydrologic applications of satellite data: 2. Flow simulation and soil water estimates, *J. Geophys. Res.*, *101*(D21), 26,527–26,538.

Habib, E., and W. F. Krajewski (2002), Uncertainty analysis of the TRMM ground validation radar-rainfall products: Application to TEFLUN-B campaign, *J. Appl. Meteorol.*, *41*, 558–572.

Hossain, F., E. N. Anagnostou, M. Borga, and T. Dinku (2004a), Hydrologic model sensitivity to parameter and radar rainfall estimation uncertainty, *Hydrol. Processes*, in press.

Hossain, F., E. N. Anagnostou, and T. Dinku (2004b), Sensitivity analyses of satellite rainfall retrieval and sampling error on flood prediction uncertainty, *IEEE Trans. Geosci. Remote Sens.*, *42*(1), 130–139.

Huffman, G. J. (1997), Estimates of root-mean-square error for finite samples of estimated precipitation, *J. Appl. Meteorol.*, *36*, 1191–1200.

Huffman, G. J., R. F. Adler, E. F. Stocker, D. T. Bolvin, and E. J. Nelkin (2003), Analysis of TRMM 3-hourly multi-satellite precipitation estimates computed in both real and post-real time, paper presented at 12th Conference on Satellite Meteorology and Oceanography, Am. Meteorol. Soc., Long Beach, Calif., 9–13 Feb.

Iguchi, T., T. Kozu, R. Meneghini, J. Awaka, and K. Okamoto (2000), Rain-profiling algorithm for the TRMM precipitation radar, *J. Appl. Meteorol.*, *39*, 2038–2052.

Liao, L., R. Meneghini, and T. Iguchi (2001), Comparisons of rain rate and reflectivity factor derived from the TRMM precipitation radar and the WSR-88D over the Melbourne, Florida, site, *J. Atmos. Oceanic Technol.*, *18*, 1959–1974.

McCollum, J. R., and R. R. Ferraro (2003), Next generation of NOAA/NESDIS TMI, SSM/I, and AMSR-E microwave land rainfall algorithms, *J. Geophys. Res.*, *108*(D8), 8382, doi:10.1029/2001JD001512.

Meneghini, R., T. Iguchi, T. Kozu, L. Liao, K. Okamoto, J. A. Jones, and J. Kwiatkowski (2000), Use of the surface reference technique for path attenuation estimates from the TRMM radar, *J. Appl. Meteorol.*, *39*, 2053–2070.

Morales, C., and E. N. Anagnostou (2003), Extending the capabilities of high-frequency rainfall estimation from geostationary-based satellite infrared via a network of long-range lightning observations, *J. Hydrometeorol.*, *4*, 141–159.

Kummerow, C., et al. (2000), The status of the Tropical Rainfall Measuring Mission (TRMM) after two years in orbit, *J. Appl. Meteorol.*, *39*, 965–982.

Kummerow, C., et al. (2001), The evolution of the Goddard Profiling Algorithm (GPROF) for rainfall estimation from passive microwave sensors, *J. Appl. Meteorol.*, *40*, 1801–1821.

Negri, A. J., and R. F. Adler (1993), An intercomparison of three satellite rainfall techniques over Japan and surrounding waters, *J. Appl. Meteorol.*, *32*, 357–373.

Negri, A. J., R. F. Adler, and L. Xu (2002), A TRMM-calibrated infrared rainfall algorithm applied over Brazil, *J. Geophys. Res.*, *107*(D20), 8048, doi:10.1029/2000JD000265.

Nijssen, B., and D. Lettenmaier (2004), Effect of precipitation sampling error on simulated hydrological fluxes and states: Anticipating the Global Precipitation Measurement satellites, *J. Geophys. Res.*, *109*, D02103, doi:10.1029/2003JD003497.

Nijssen, B., G. M. O'Donnell, D. P. Lettenmaier, D. Lohmann, and E. F. Wood (2001), Predicting the discharge of global rivers, *J. Clim.*, *14*, 3307–3323.

O'Donnell, G., K. P. Czajkowski, R. O. Dubayah, and D. P. Lettenmaier (2000), Macroscale hydrological modeling using remotely sensed inputs: Application to the Ohio River Basin, *J. Geophys. Res.*, *105*(D10), 12,499–12,516.

Quinn, P. F., K. J. Beven, P. Chevallier, and O. Planchon (1991), The prediction of hillslope flow paths for distributed hydrological modeling using digital terrain models, *Hydrol. Processes*, *5*, 59–79.

Quinn, P. F., K. J. Beven, and R. Lamb (1995), The ln (*a*/tan *b*) index: How to calculate it and how to use it in the TOPMODEL framework, *Hydrol. Processes*, *9*, 161–182.

Rhoads, J., R. Dubayah, D. P. Lettenmaier, and G. O'Donnell (2001), Validation of land surface models using satellite-derived surface temperature, *J. Geophys. Res.*, *106*(D17), 20,085–20,099.

Smith, E. A. (2001), Satellites, orbits and coverages, paper presented at IGARSS 2001 (International Geoscience and Remote Sensing Symposium), Inst. of Electr. and Electron. Eng., Sydney, N. S. W., Australia, 9–13 July.

Todd, M. C., C. Kidd, D. Kniveton, and T. Bellerby (2001), A combined satellite infrared and passive microwave technique for estimation of small-scale rainfall, *J. Atmos. Oceanic Technol.*, *18*, 742–756.

Tsonis, A. A., G. N. Triantafyllou, and K. P. Georgakakos (1996), Hydrological applications of satellite data: 1. Rainfall estimation, *J. Geophys. Res.*, *101*(D21), 26,517–26,525.

Winchell, M., H. V. Gupta, and S. Sorooshian (1998), On the simulation of infiltration- and saturation excess runoff using radar-based rainfall estimates: Effects of algorithm uncertainty and pixel aggregation, *Water Resour. Res.*, *34*, 2655–2670.

Xu, L., G. Xiaogang, S. Sorooshian, P. A. Arkin, and B. Imam (1999a), A microwave infrared threshold technique to improve the GOES precipitation index, *J. Appl. Meteorol.*, *38*, 569–579.

Xu, L., S. Sorooshian, G. Xiaogang, and H. V. Gupta (1999b), A cloud-patch technique for identification and removal of no-rain clouds from satellite infrared imagery, *J. Appl. Meteorol.*, *38*, 1170–1181.

E. N. Anagnostou and F. Hossain, Department of Civil and Environmental Engineering, University of Connecticut, 261 Glenbrook Road, U 2037, Storrs, CT 06269, USA. (manos@engr.uconn.edu)